RESEARCH ARTICLE

Dielectric Relaxation and Suitability of Scaling parameters study on $Mn_{0.7+x}Zn_{0.3}Si_xFe_{2-2x}O_4$ (x = 0.0 - 0.3) Ferrites

Nimish H. Vasoya[1], Kiran G. Saija[2], Akshay R. Makadiya[3], Tushar K. Pathak[4], Urmila M. Meshiya[3], Pooja Y. Raval[3], Kunal B. Modi[3,*]

[1]Department of Balbhavan, Children's University, Sector-20, Gandhinagar 382021, India
[2]Smt. R.P.Bhaloida Mahila College, Upleta 360490, India
[3]Department of Physics, Saurashtra University, Rajkot 360005, India
[4]Department of Physics, Government Engineering College, Kankot, Rajkot 360005, India

*Correspondenc author: E-mail: kunalbmodi2003@yahoo.com

DOI: 10.5185/amlett.2020.121587

The compositional dependence of the real (ε') and imaginary (ε'') parts of complex dielectric permittivity (ε*) and loss tangent (tan δ) for $Mn_{0.7+x}Zn_{0.3}Si_xFe_{2-2x}O_4$ (x = 0.0, 0.1, 0.2 and 0.3) spinel ferrite series was investigated over wide frequency (f = 20 Hz to 1 MHz) and temperature (T = 300 K to 673 K) ranges. Frequency dependence of ε',ε'' and tan δ has been explained based on the two-layer model of dielectrics. The nonlinear relationship between ε'(f) and σ'(f) suggests multi-relaxation process and formation of a broad hump in ε'(f, T) plots indicates collective contributions from electrons and holes to the polarization. The scaling by normalized frequency (f/f_c) and scaled frequency (f/σ_{dc}) are found successful for ε' in high-frequency regime only while scaling found successful for ε'' over the whole range of frequency. The suitability of various scaling parameters was also tested for the master curve generation. The co-existence of localized and delocalized relaxations is verified.

Introduction

For eight decades,a study on physical properties of spinel structured ferrites in single-crystalline, polycrystalline, nanocrystalline, thin/thick films, composites forms are subject of interest from fundamental and applied research point of view. These compounds possess a very interesting combination of high values of dc resistivity, dielectric permittivity, permeability, magnetization, thermal stability along with low eddy current loss, and low dissipation. These peculiarities make them suitable for high-frequency applications. The dielectric properties are decisively dependent on the synthesis route employed, preparative parameters, type of substituted metallic cations, etc. Besides, magnetic ferrites possess other advantages such as ease of preparation in bulk quantity, cost-effectiveness with a very high reproduction rate [**1**].

Among the wide range of ferrite families, two spinel structured series, $Ni_{1-x}Zn_xFe_2O_4$,and $Mn_{1-x}Zn_xFe_2O_4$ with x = 0.0 to 1.0, have demonstrated potentiality for their usage in high-frequency low loss applications since long. This includes biomedical applications, transformer cores, telecommunications, information storage, sensors, magnetic fluids, inductors, hyperthermia applications, etc. [**2**]. Taking into account, magnetic, electric, and dielectric characteristics discussed above essential for such applications, the Mn-Zn ferrites system in general and a typical composition, $Mn_{0.7}Zn_{0.3}Fe_2O_4$, in particular, found promising [**1**]. At the same time, silica (SiO_2) is one of the substituents that are to be regulated meticulously. Considering the ionic radius (0.40 Å), oxygen affinity (-614.5 kJ/mol) and concentration, the probability of Si^{4+} ions tobe segregated at grain boundaries is quite high as compared to very large Mn^{2+} ions having an ionic radius of 0.83 Å and very small oxygen affinity of the order of – 215.5 kJ/mol [**3**]. These peculiarities motivated us to synthesize and investigate the physical properties of Mn^{2+}-Si^{4+}ions co-substituted for Fe^{3+} ions in order to maintain charge neutrality in $Mn_{0.7}Zn_{0.3}Fe_2O_4$ ferrite composition with common chemical formula, $Mn_{0.7+x}Zn_{0.3}Si_xFe_{2-2x}O_4$ with x = 0.0, 0.1, 0.2 and 0.3,in a systematic manner.

Dielectric spectroscopy is referred to as one of the most versatile experimental techniques. This is based on the fact that though primary dielectric parameters, real part (ε') of complex dielectric permittivity (ε^*) and the dielectric loss tangent (tan δ) or dissipation factor (D) are used to determine various formalism such as complex electric modulus (M^*), complex impedance (Z^*), complex admittance (Y^*), and complex electric conductivity (σ^*), each one will provide distinct information concerning to materials characteristics. This includes conduction mechanism, dielectric polarization, dielectric relaxation phenomena, relaxation frequencies, relaxation times, activation energy values, grain and grain boundary resistances and capacitances, electrode effect, etc. [**4-10**].

The term dielectric relaxation implies the alteration of the electric polarization following the application of an electric field to a sample. The long-range or delocalized relaxation could be recognized on account of fast polarization in which all or many molecules of the system that are electrically active are participating. On the other hand, the localized polarization would be the relaxation of one or a few molecules. Overlapping or non-overlapping of the peak positions of the $Z''(f)/Z''_{max}$ and $M''(f)/M''_{max}$ versus frequency plot decides the presence of non-localized relaxation and/or localized relaxation in the system. Alternatively, other formalisms are also employed to identify the type of relaxation that exists. In the course of experimental data analysis, scaling or single 'master curve' generation is a principal aspect since a system that exhibits scale-independent characteristics land themselves to the streamlined and frequently universal description. In order to understand various physical phenomena, constructing a 'master curve' is indispensable as it carries more details as compared to any single temperature run. Not only that as the density of data points is substantially greater in the master curve than on the single temperature runs, but it also improves the authenticity of the derived information.

Restricted to recent (2016-2020) reports on dielectric properties of $Zn_xMn_{1-x}Fe_2O_4$ (x = 0.0 to 1.0) spinel ferrites synthesized by solid-state reaction method [**11-12**], sol-gel route [**13**], combustion process [**14**], microwave-induced urea-nitrate process [**15**] are available in the literature. On the other hand, divalent Cr^{2+}-substituted ferrites, $Mn_{0.5}Zn_{0.5-x}Cr_xFe_2O_4$ (x = 0.0, 0.3 and 0.5) [**16**] and cobaltites, $Mn_{0.5}Zn_{0.5-x}Cr_xCo_2O_4$ (x = 0.0, 0.3 and 0.5) [**17**], trivalent cation Gd^{3+} - substituted $Mn_{0.5}Zn_{0.5}Gd_xFe_{2-x}O_4$ prepared by facile coprecipitation method [18] and chemical co-precipitation route [**19**], Nd^{3+}-substituted $Mn_{0.5}Ni_{0.1}Zn_{0.4}Gd_xFe_{2-x}O_4$ (x = 0.0 to 1.0) synthesized by usual double ceramic method [**20**] as well as Sm^{3+} – Gd^{3+} co-substituted $Mn_{0.4}Zn_{0.6}Sm_xGd_yFe_{2-(x+y)}O_4$ system prepared by microwave hydrothermal route [**21**] and tetravalent titania (Ti^{4+}) ions substituted $Mn_{0.5}Zn_{0.5}Ti_xFe_{2-4/3x}O_4$ (x = 0.0 to 0.5) prepared by hydrothermal method [**22**] have been reported. Couple of research articles describing dielectric behaviour of $Mn_{0.4}Zn_{0.6}Fe_2O_4$ + $Co_{0.4}Zn_{0.6}Fe_2O_4$ composites [**23**] and $CaCu_3Ti_4O_{12}$ (0.0 to 0.5 wt %) doped Mn-Zn ferrites [**24**] are also available.

Concentrating on impact of non-magnetic, tetravalent Si^{4+} ions substitution on various physical properties of spinel ferrite series not necessarily Mn-Zn ferrite based system and irrespective of time span, few reports are accessible in the literature. The effect of SiO_2 on structural and dielectric properties of $Mn_{0.5}$ $Ni_{0.5}Fe_2O_4$ ferrite has been studied by Saadon *et. al.,* [**25**]. The magnetic properties of Si^{4+}/ Ti^{4+} substituted $Cd_{0.5}Co_{0.5+t}A_tFe_{2-2x}O_4$ (A = Si or Ti and t = 0.0 to 0.4) prepared by ceramic processing have been investigated by Patil *et. al.,* [**26**]. The influence of 0.5 wt % Si as an additive on the dielectric behavior of Cu-Zn and Ni-Zn ferrites has been reported by Uzma *et. al.,* [**27,28**]. The effect of nano-SiO_2 (10 nm) on magnetic and dielectric properties of $Li_{0.3}Zn_{0.4}Fe_{2.3}O_4$ has been studied by Mahmoudi *et al.* [**29**]. The influence of amorphous silica matrix on structural, magnetic and dielectric properties of $(CoFe_2O_4)_{1-y}$ / $(SiO_2)_y$ nano-composites have been investigated by Nadeem *et. al.,* [**30**]. Similarly, the electrical properties of Si^{4+} ion substituted $CuFe_2O_4$ [**31**], lithium ferrite [**32,33**] and cobalt ferrite [34] are also available in the literature.

Over the last few years, we have investigated dielectric properties of spinel ferrite system, $Mn_{0.7+x}Zn_{0.3}Si_xFe_{2-2x}O_4$ (x=0.0-0.3) (f = 20 Hz to 1 MHz) (T = 300K to 673K) in the form of complex electric modulus (M^* = M' + jM''), complex ac conductivity (σ^* = σ' – σ'') and complex impedance (Z^* = Z' – iZ'') spectroscopy [**8-10**]. The high field magnetization, thermal variation of low field ac susceptibility and dc resistivity has been studied for the same system very recently [**35**]. In the present study, primary dielectric parameters, ε', ε'', and tanδ, are studied as a function of composition, frequency, and temperature. The suitability of various scaling parameters is tested to construct a single 'master curve'. The polarization and dielectric relaxation are discussed in detail.

Experimental details

The complete experimental details concerning to synthesis of spinel ferrite series, $Mn_{0.7+x}Zn_{0.3}Si_xFe_{2-2x}O_4$ (x = 0.0, 0.1, 0.2 and 0.3) by the usual double sintering ceramic method, crystal structure and structural parameters determination by means of Rietveld refinement of X-ray powder diffraction patterns and dielectric measurements as a function of composition, frequency and temperature are given in [**8-10**].

Results and discussion

The frequency (f) dependent plots of the real part (ε') and an imaginary part (ε'') of complex dielectric permittivity (ε^* = ε' - jε'') at several temperatures (T) are displayed in **Fig. 1** and **Fig. 2**. It is seen that ε' and ε'' decrease with an increase in f. In low- frequency regime ε' and ε'' decrease rapidly, in high-frequency regime they decrease slowly and become independent of f at a much higher frequency. Polycrystalline ferrites comprised of well-conducting grains segregated by highly resistive grain boundaries (Maxwell-Wagner brick layer model) [**36**]. The difference between grain resistance (R_g) and grain boundary resistance (R_{gb}), where $R_{gb} >> R_g$ results in interfacial polarization responsible for dielectric properties of semiconducting ferrites. Electrons arrived at grain boundaries via hopping mechanism, if grain boundary resistance is sufficiently high, electrons piled up at grain boundaries and give rise to polarization. On increasing f, electrons reverse the direction of motion more frequently. Thus, the probability of electrons reaching grain boundaries decreases, and consequently polarization also

decreases. Accordingly, ε' decreases with *f*. Alternatively, ε'(*f*) variation can be explained as follows. In low-frequency regime, ω (= $2\pi f$) << $1/\tau$ (τ is the relaxation time) free electric dipoles obey the alternating field and ε' = ε_s (value of ε' at quasistatic fields). On increasing *f* for which $\omega < 1/\tau$, dipoles commence to fall behind the field and ε' decreases moderately. As soon as *f* reaches the characteristic frequency with $\omega = 1/\tau$, ε' drops i.e. relaxation process occurs. In the high-frequency region $\omega >> 1/\tau$ and dipoles can no longer follow the field, thus ε' = ε_∞ (high-frequency value of ε'). In a qualitative manner,the same characteristics have been demonstrated by the system.

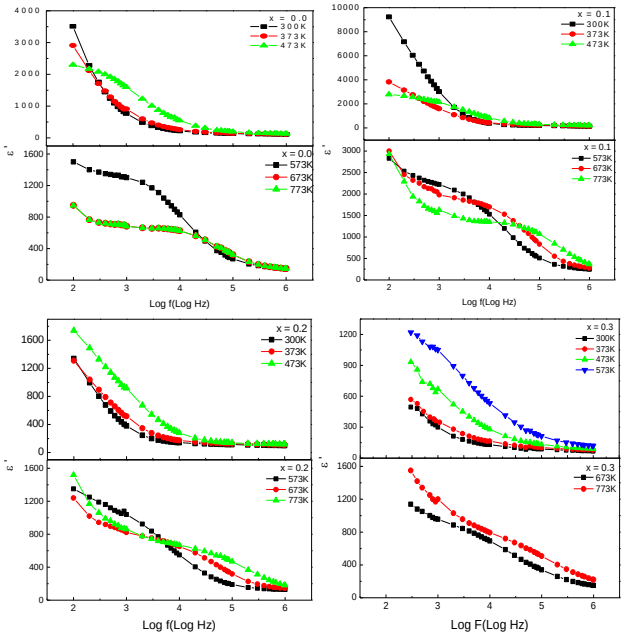

Fig. 1. Variation of dielectric constant (ε′) with frequency at different temperatures for *x* = 0.0, 0.1, 0.2 and 0.3 compositions.

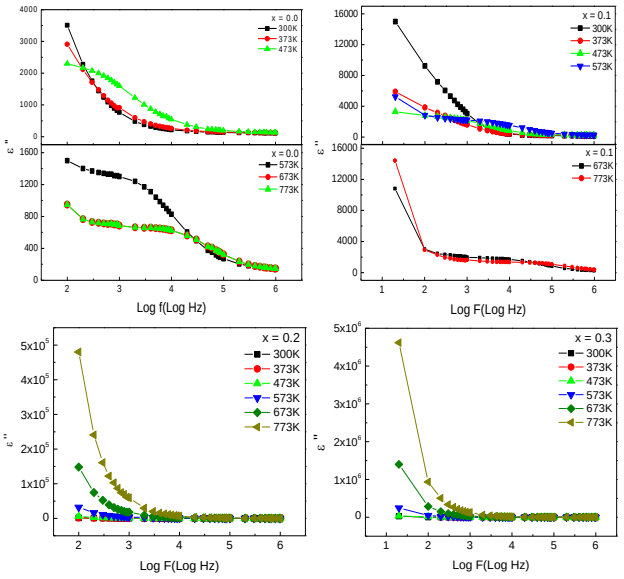

Fig. 2. Frequency dependence of ε′′at different temperatures for *x* = 0.0, 0.1, 0.2 and 0.3 compositions.

A close examination of figure 1 unveils that for *x* = 0.0 - 0.2 compositions at $T \geq 573$ K and for *x* = 0.3 composition at $T \geq 673$ K broad hump has been observed and that shifted to higher frequency side on increasing temperature. This implies that such hump is associated with a relaxation process activated thermally. Impedance spectral analysis has shown that grain boundary resistance increases for *x* = 0.1 to 0.2 compositions and is maximum for *x*=0.2 composition that supports maximum segregation of Si^{4+} ions at grain boundaries and for *x*=0.3 composition, large fraction of Si^{4+} ions enters into grains and thereby decreases the grain boundary resistance [**8-10**]. As a result, polarization is expected to decrease for *x* = 0.3 composition and more thermal energy is required to enhance the polarization process contributed by electrons and holes. Thus, for *x* = 0.0 to 0.2 compositions broad hump occurs at $T \geq 573$ K and for *x* = 0.3 composition broad maximum occurs $T \geq 673$ K. The presence of hump in ε'(*f*) plots is rather unanticipated. As reported by Rezlescu*et al.* [**37**], when two types of charge carriers, electrons (*n*) and holes (*p*), collectively contribute to the polarization such hump may be expected in ε'(*f*) curves.According to Perfenov and Nazipov [**38**], when spinel ferrites synthesized without specifically controlled conditions (for example, preparation in oxygen at elevated pressure), they contain oxygen vacancies, which leads to a partial reduction of ferric ion (Fe^{3+}) into ferrous ion (Fe^{2+}). Here, ferrous ions act as donor impurity relative to ferric ions, which leads to n-type conductivity by electron (e^-) exchange mechanism : $Fe^{2+} \leftrightarrow Fe^{3+} + e^-$. In order to maintain charge neutrality some of the Mn^{2+} ions get converted into Mn^{3+} ions, which leads to p-type conductivity by hole (e^+) exchange mechanism : $Mn^{2+} + e^+ \leftrightarrow Mn^{3+}$. The p-type can also be described by the exchange of holes among Fe^{3+} and Fe^{4+} ions according to $Fe^{4+} \leftrightarrow Fe^{3+} + e^+$ mechanism, but in spinel structured ferrite materials Fe^{4+} ions do not occur [**38**]. Likewise, e^+ can transfer among Fe^{3+} and Fe^{2+} by $Fe^{3+} \leftrightarrow Fe^{2+} + e^+$ process. For such a p-type conduction mechanism, the concentration of ferrous ions should much exceed the concentration of ferric ions in the system. But in this case, associated oxygen non-stoichiometry is too large for ferrites and single-phase crystal structure formation, as in the present case, can not be sustained. The contribution from holes is falling short as compared to that received from the exchange of electron and has the opposite sign. Besides, because the mobility of holes is lower than that of electrons their contribution to polarization decreases more swiftly. Theoretically by quantum computations of allowed bands energy and experimentally from the Hall coefficient and the resistivity of the material it is suggested that the mass of holes is greater than the mass of electrons. The mobility (μ) of the charge carriers (electrons and holes) being inversely proportional to the mass of the charge carriers, $\mu = (q/m).\tau$ (τ, the time between two collisions and q , the charge of carrier), the mobility of holes is lower than that of electrons. When the

electric field (Ê) is applied to the semiconducting ferrite it will start to conduct electric current by the motion of charge carriers. The carriers accelerate into the Ê and deaccelerate by different scattering mechanisms. The average drift velocity (V_d) is directly proportional to the Ê given by : $V_d = \mu\hat{E}$. Thus, electrons and holes respond differently to Ê [**39**]. By summing up the contributions from electrons and holes to the polarization process, one can foresee $\varepsilon'(f)$ behavior as shown in **Fig. 3**. In $\varepsilon''(f, T)$ curves of x = 0.0 and x = 0.1compositions similar wide hump has been noticed for $T \geq$ 573K and $T \geq$ 673 K respectively. The position of hump shifted towards the high-frequency side without significant change in intensity on increasing temperature. This advice that charge carrier concentration remains unaffected by thermal activation [**40**].

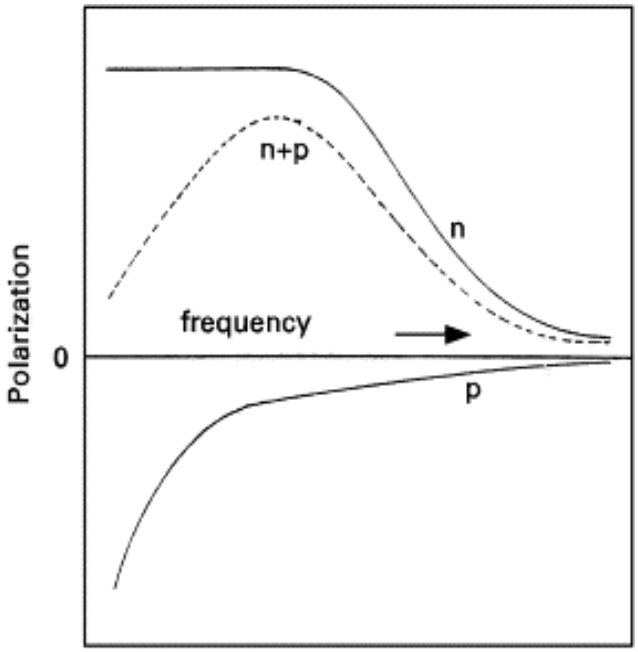

Fig. 3. Contributions of *n*-type and *p*-type charge carriers to polarization (Rezlescu model).

The loss tangent (tan $\delta = \varepsilon''/\varepsilon'$) against frequency plots registered at different temperatures are shown in **Fig. 4**. Mostly, tan δ decreases with f, which means dielectric losses are much higher in the low-frequency region than those occurring in the high-frequency regime. Such behavior of tan δ is associated with losses by a conduction process (relaxation mechanism) [**41**]. Interestingly, for x = 0.0 – 0.2 compositions, tan δ (f, T) plots show broad peak for $T \leq$ 373K (**Fig. 4**). Whenever hopping frequency of electron between ferrous (Fe^{2+}) and ferric (Fe^{3+}) ions or hole among Mn^{2+} and Mn^{3+} ions at the octahedral (B-) sites is equivalent to f and the condition ωτ = 1gets satisfied, maximum electrical energy is transferred to oscillating ions and power losses shoot up that results in resonance peak. The reduction in peak intensity with temperature indicates a decrease in charge carriers by thermal activation.

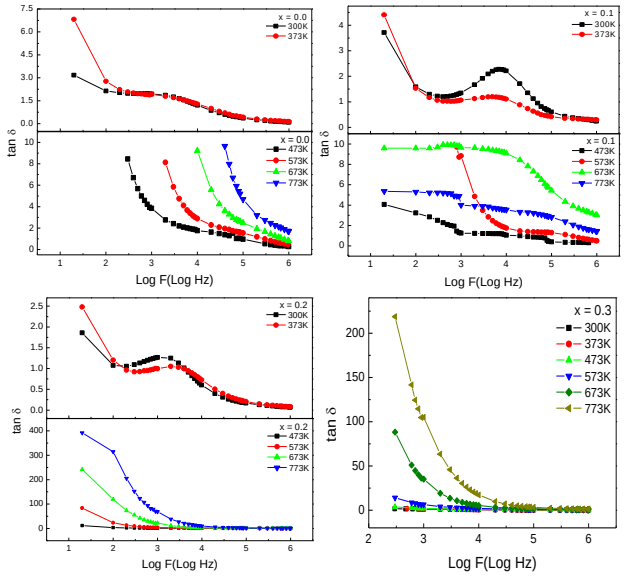

Fig. 4. Variation of loss tangent (tanδ) with frequency at different temperatures for x = 0.0, 0.1, 0.2 and 0.3 compositions.

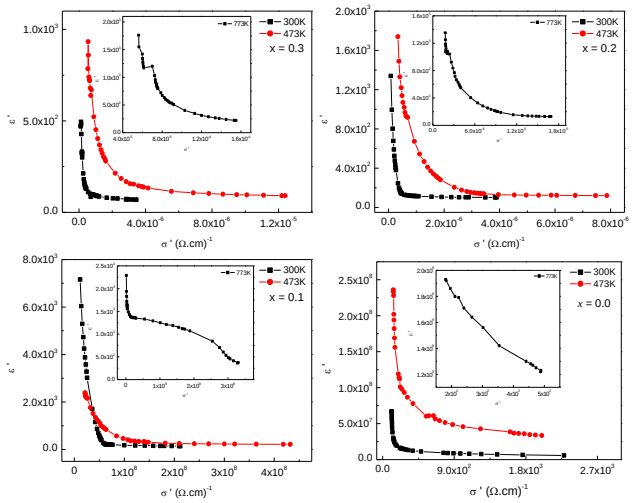

Fig. 5. The relationship between ε′ and σ′ at selected temperatures for different ferrites.

In **Fig. 5**, $\varepsilon'(f)$ versus $\sigma'(f)$ [**9**] plots at several temperatures do not show a straight line, suggest a poly-dispersive/multi relaxation process clearly demonstrated in Nyquist plots [**10**]. The ε'' against ε' plots (Cole-Cole plots) for x = 0.0 – 0.2 compositions are shown in **Fig. 6**. Indication of semi-circle formation is observed for x = 0.1 and x = 0.2 compositions at $T \leq$ 373K only. On the other hand, for all the compositions for T> 373K, the plots show spike-like nature suggests existence and high influence of DC conductivity in the studied ferrites. Appertaining to the above observations, it is concluded that for the ferrite materials under investigation ε^* presentation is not suitable representation. Basically, this Cole-Cole plot or complex Argand plane plot is one of the most convenient ways of verifying the poly-dispersive nature of dielectric relaxation in the system. In the case of the pure mono-dispersive Debay process, one expects semicircular

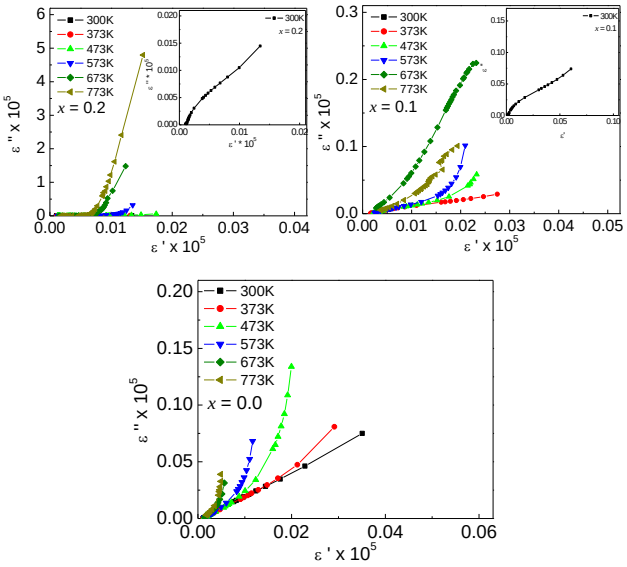

Fig. 6. Cole – Cole plots for x = 0.0, 0.1 and 0.2 compositions at several temperatures.

arc with a center located on the ε'-axis. On the contrary, for the poly-dispersive relaxation process, Argand plots are close to circular arcs, with endpoints on the real ε'-axis and center lie below this axis (**Fig. 7**). In these circumstances, ε^* is known to be described by the empirical relation: $\varepsilon^* = \varepsilon_\infty+(\varepsilon_s- \varepsilon_\infty)/1+(i\omega\tau)^{1-\alpha}$. Here α is the measure of the distribution of relaxation times and α = 0 for the mono-dispersive Debye process. The parameter α determined from the angle subtended by the radius of the circle with the ε'-axis is found to be 0.22 for x = 0.1 and x = 0.2 compositions at T = 373 K (**Fig. 7**), confirms poly-dispersive nature of dielectric relaxation.

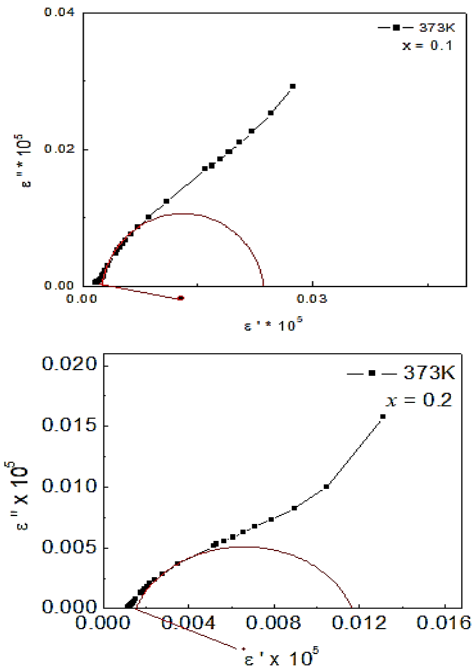

Fig. 7. Complex Argand plane plots between ε″ and ε′ at 373 K for the typical compositions with x = 0.1 and 0.2.

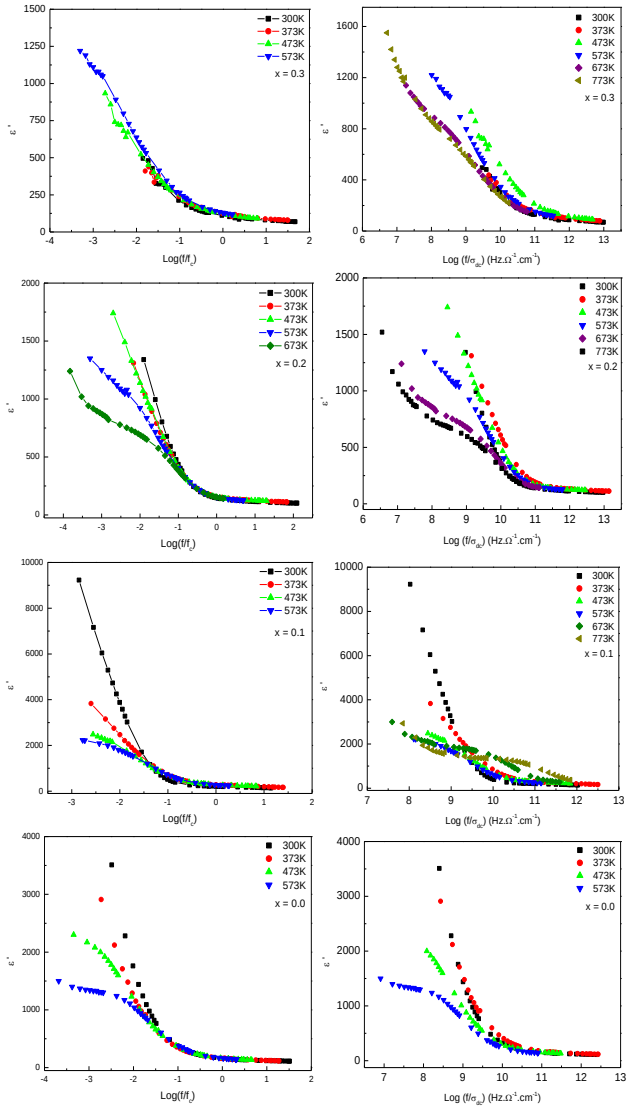

Fig. 8. ε′ master curve of all the four investigated compositions of spinel ferrite system, $Mn_{0.7+x}Zn_{0.3}Si_xFe_{2-2x}O_4$.

The ε' and ε'' scaled as a function of normalized frequency (f/f_c) ($f_c \sim f_{max}$ is determined from M', $M''(f,T)$ plots [**8**]) and scaled frequency (f/σ_{dc}) (σ_{dc}, DC conductivity value [**6**]) at different temperature are illustrated in **Fig. 8** and **Fig. 9**. It is seen that scaling of ε' is successful in the high-frequency region only ($f > f_c$). The failed master curve generation for ε' in the low-frequency region ($f < f_c$) was reported by Saafan *et. al.*, [**42**] for Al^{3+} substituted Mn-Zn ferrites. However, satisfactory scaling was observed for ε" by using both f_c and σ_{dc}. These led to a remarkable equivalency between f_c and σ_{dc} as already suggested by Sidebottom *et. al.*, [**43**]. The unsuccessful scaling of ε' for $f < f_c$ is attributed to the existence of holes as minority charge carriers in the materials whose thermal dependence cannot be eradicated by scaling *f*either by f_c or σ_{dc}. This is quite expected due to the fact that σ_{dc} and f_c are characteristic values related to the motion of electrons and do not involve a contribution from holes [**42**].

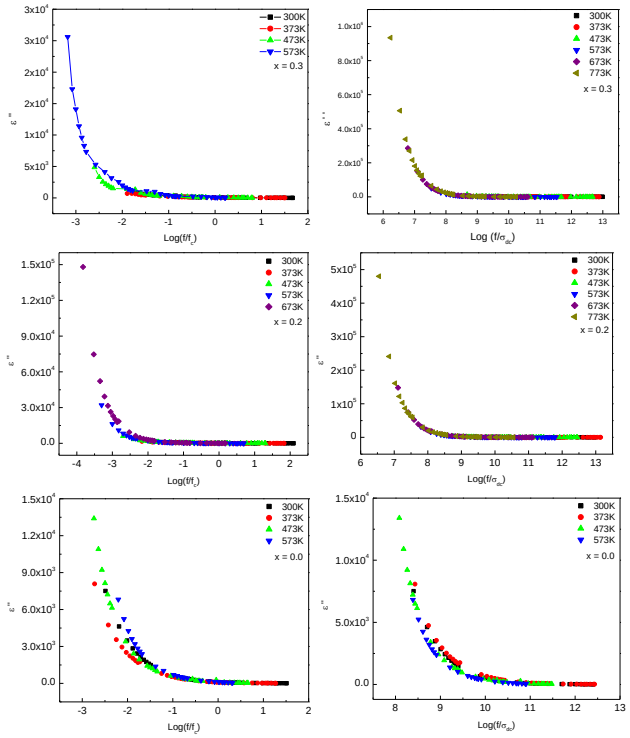

Fig. 9. ε′′ master curve of selected compositions (x = 0.0, 0.2 and 0.3) recorded at different temperatures.

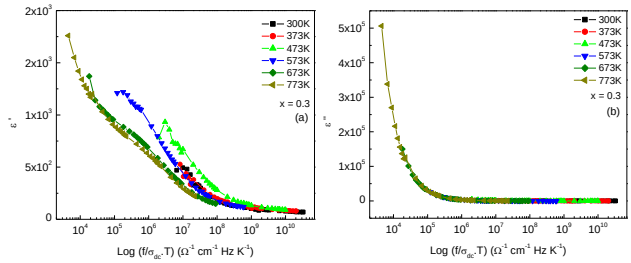

Fig. 10. Scaling curves of (a) real part of dielectric permittivity(b) imaginary part of dielectric permittivity and (c) conductivity at different temperatures for the typical composition with x = 0.3 scaled by the scaling law in the form suggested by Roling et. al., [45].

The thermoelectric power measurements carried out on the system, $Mn_{0.7+x}Zn_{0.3}Si_xFe_{2-2x}O_4$, suggest that the conduction is because of electron exchange between Fe^{2+} and Fe^{3+} ions at the octahedral sites of the spinel lattice [**44**]. At the same time, observed hump in $\varepsilon'(f, T)$ plots (Figure 1) suggests a collective contribution from holes and electrons to polarization (Figure 3). Thus, it seems that the motion of positive charge carriers (holes) as minority charge carriers or polaron hopping not revealed in σ_{dc} values is the responsible factor for the unsuccessful master curve generation. An attempt has been made to scale the frequency axis by the $\sigma_{dc}T$ parameter (i.e. $f/\sigma_{dc}T$) as suggested by Rolling *et. al.*, [**45**]. **Fig. 10** shows $\varepsilon'(f, T)$ and ε'' (f, T) curves scaled by $\sigma_{dc}T$ for the typical composition with x = 0.3. It is found that scaling of the frequency axis by $\sigma_{dc}T$ does not upgrade the quality of the master curve when compared with the curves scaled by σ_{dc} only (i.e. f/σ_{dc}) (Figures 8 and 9). On the similar line, permittivity data, $(\varepsilon' - \varepsilon_\infty)/\Delta\varepsilon$, is scaled by $(f/\sigma_{dc}T)$ and $(f.\Delta\varepsilon.\varepsilon_0/\sigma_{dc})$ and same are displayed in **Fig. 11** for the selected composition (x = 0.3). In the presentation permittivity difference $\Delta\varepsilon$ is given by $\varepsilon_s - \varepsilon_\infty$, where ε_s and ε_∞ are the lowest frequency and highest frequency dielectric permittivity value. The observed failure in master curve generation is owing to the fact that $\Delta\varepsilon$ which relies on temperature, mobile charge carrier concentration, and the hoping distance is not constant, which is a fundamental need for successful application of this scaling law [**46**].

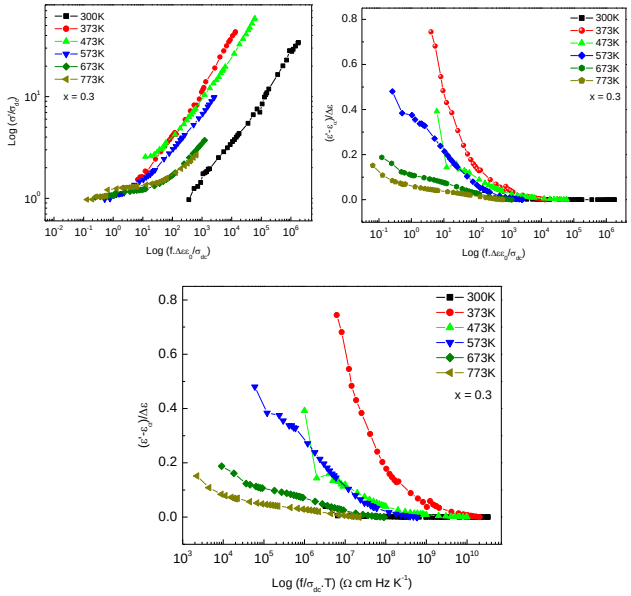

Fig. 11. The master curves of the conductivity and the permittivity of the typical composition with x = 0.3 recorded at different temperatures by the scaling law in the form suggested by Roling et. al., [45].

A comparative study between impedance, electric modulus and loss factor permits a straightforward explanation of the microscopic processes accountable for the recorded a.c response [**47**]. Shown in **Fig. 12**, the variation of normalized parameters of loss tangent (tan δ/tan δ_{max}) and electric modulus (M''/M''_{max}) [**8**] as a function of normalized frequency (f/f_{max}) registered at T=300K for x = 0.0 to 0.3 compositions. Such a coupled plot is competent to discriminate the predominance of non-localized (i.e. long-range conductivity) and localized (i.e. dielectric relaxation) movement of charge carriers in a relaxation process. The observed non-overlapping of peak frequencies between M''/M''_{max} and tan δ/tan δ_{max} suggest that the relaxation process is mainly governed by the short-range movement of charge carriers and departs from an ideal Debye type behavior. On the other hand, the coincidence of peak frequencies indicates that long-range movement of charge carriers is dominant [**47,48**]. The observed small mismatching of the peak frequencies indicates a non-Debye type behavior and the simultaneous presence of the components from both long-range and localized conduction responsible for dielectric relaxation in the system.

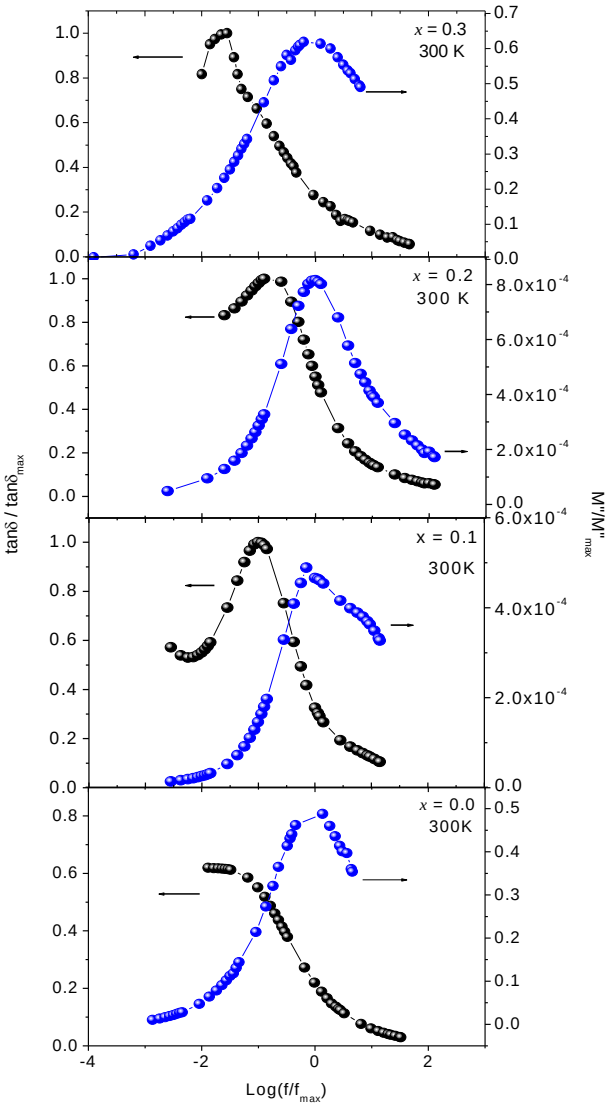

Fig. 12. Normalized frequency dependent normalized loss tangent and electric modulus for $Mn_{0.7+x}Zn_{0.3}Si_xFe_{2-2x}O_4$ system with x = 0.0 to 0.3 compositions registered at 300 K.

Conclusions

A comprehensive investigation on the variation of dielectric parameters (ε', ε'' and tan δ) as a function of composition (x = 0.0 – 0.3), frequency (f = 20 Hz – 1 MHz) and temperature (T = 300 K – 673 K) for spinel ferrite system, $Mn_{0.7+x}Zn_{0.3}Si_xFe_{2-2x}O_4$, leads to conclude that (a) the dispersion characteristic of ε', ε'' and tan δ can be explained on the basis of two-layer model (b) the observed hump in $\varepsilon'(f, T)$ plots and unsuccessful process of master curve generation by σ_{dc} and $\sigma_{dc}T$ as scaling parameters suggest the collective contributions from electrons and holes to the polarization (c) the occurrence of poly-dispersive relaxation process has been confirmed by $\varepsilon'(f)$ versus $\sigma'(f)$ plot (d) the ε* presentation is not suitable to represent dielectric data of ferrites (e) the scaling process by f/f_c and f/σ_{dc} is found successful for ε′ in the high-frequency region only while it is successful for ε” in the whole range of frequency while scaling by $\sigma_{dc}T$ does not show any improvement in master curve generation (f) the non-overlapping of peak position in tan δ/tan δ_{max} and M''/M''_{max} against f/f_{max} plots is evidence of the components from localized relaxation and delocalized relaxation.

Keywords

Ferrites, dielectric properties, dielectric relaxation, scaling.

Received: 28 April 2020
Revised: 12 June 2020
Accepted: 17 July 2020

References

1. Alex Goldman, “Modern ferrite technology”, 2nd Edition, Springer, USA, **2006**.
2. Thakur, P.; Taneja, S.; Sindhu, D.; Luders, U.; Sharma, A.; Ravelo, B.; Thakur, A.; *J.Super. Nov. Mag.*, DOI: 10.1007/s 10948-020-05489-z.
3. Pint,B. A.; Alexander, K. B.; *J. Electrochem. Soc.*,**1998**, 145, 1819.
4. Hcini, F.; Hcini, S.; Alzahrani, B.; Zemni, S.; Bouaziz, M. L.; *Appl. Phys. A*, **2020**, *126*, 362.
5. Shridhar, Ch. S. L. N.; Laxmi, K. S. S.M.; Potukuchi, D. M. Lakshmi, Ch. S.; *Mater. Res.Exp.*, **2020**, *6*, 126117.
6. Patil, A. D.; Algude, S. G.; Shirsath, S. E.; Jadhav, S. S.; Patange, S. M.; *Phase Trans.*, **2019**, *92(9)*, 790.
7. Zaki, H.; Engineering magnetic, dielectric and microwave properties of ceramics and alloys, **2019**, *57*, 113.
8. Vasoya, N. H.; Jha, P. K.; Saija, K. G.; Dolia, S. N.; Zankat, K. B.; Modi, K. B.; *J. Elect.Mater.*, **2016**, *45*, 917.
9. Vasoya, N. H.; Jha, P. K.; Saija, K. G.; Bhalodia, J. A.; Modi, K. B.; *J. Adv. Diel.*, **2017**, *7*, 1750022.
10. Vasoya, N. H.; Saija, K. G.; Dolia, S. N.; Jha, P. K.; Modi, K. B.; *Mater. Res. Exp.*, **2017**, *4*, 16301.
11. Arais, A. A.; Rady, K. E.; Shams, M. S.; *Bulg. J. Phys.*, **2018**, *45*, 44.
12. Yusmar, A.; Armitasari, L.; Suharyadi, E.; *Mater. Today Proc.*, **2018**, *5*, 14955.
13. Rahman, A.; Abdullah, H.; Zulfakar, M. S.; Singh, M. J.; Islam, M. T.; *J. Sol-Gel Sci.Technol.*, **2016**, *77*, 470.
14. Bharamagoudar, R. C.; Angadi, J.; Patil, A. S.; Kankanawadi, L. B.; Mathad, S. N.; *Int. J. Self Prop. High Temp. Synth.*, **2019**, *28*, 132.
15. Maleknejad, Z.; Gheisari, Kh.; Honarbaksh Raoul, A.; *J. Supercond. Nov. Magn.*, **2016**, *29*,2523.
16. Choudhary, P.; Tyagi, T.; Dar, M. A.; Varshney, D.; *AIP Conf. Proc.*, **2016**, *1731*, 09008-1.
17. Yadav, A.; Dar, M. A.; Choudhary, P.; Shah, P.; Varshney, D.; *AIP Conf. Proc.*, **2016**, *1728*, 020301-1.
18. Phor, L.; Kumar, V.; *J. Adv. Ceram.*, **2020**, *9*, 243.
19. Tanbir, K.; Ghosh, M. P.; Singh, R. K.; Mukherjee, S.; *J. Mater. Sci.*, **2020**, *31*, 3529.
20. Agami, W. R.; *Phys. B.*, **2018**, *534*, 17.
21. Jagadeesha Angadi, V.; Rudraswamy, B.; Sadhana, K.; Praveena, K.; *Mater. Today Proc.*, **2016**, *3*, 2178.
22. Sridhar, Ch. S L N; Siva Maha Laxmi, K. S.; Potukuchi, D. M.; Lakshmi, Ch Sanyasa; *Mater. Res. Exp.*, **2020**, *6*, 126117.
23. Ragini, S.; Bharadwaj, S.; Burnwal, S. K. Murthy, S. R.; *Int. J. Appl. Eng. Res.*, **2018**, *13*, 4538.
24. Wu, G.; Yu, Z.; Sun, K.; Guo, R.; Jiang, X.; Wu Ch.; Lan, Zh.; *J. Mag Mag Mater.*, **2020**, *513*, 167095.
25. Saadon, A. K.; Al-Haitham, Ibn; *J. Pure Appl. Sci.*, **2012**, *25*, 186.
26. Patil, S. A.; Mahajan, V. C.; Patil, M. G.; Ghatage, A. K.; Lotke, S. D.; *J. Mater Sci.*, **1999**, *34*,6063.
27. Uzma, G.; *Chinese Phys. B*, **2014**, *23*, 057502.
28. Uzam G.; *Indian J. Pure Appl. Phys.*, **2015**, *53*, 271.
29. Mahmoudi, M.; Kavanlouei, M.; *Int. J. Mater. Res.*, **2014**, *105*, 1097.

30. Nadeem, K.; Zeb, F.; Azeem Abid,M.; Mumtaz, M.; Anis ur Rehman, M.; *J. Non Cryst. Solids*, **2014**, *400*, 45.
31. Patil, B. L.; Sawant, S. R.; Patil, S. A.; Patil, R. N.; *J. Mater. Sci.*, **1994**, *29*, 175.
32. Verma, V.; Pandey, V.; Kotnala, R. K.; Kishan,Hari; Kumar, N.; Kothari, P. C.; *J. Alloys Compd.*, **2007**, *443*, 178.
33. Mazen, S. A.; Abu-Elsad, N. I.; *J. Magn. Magn. Mater.*, **2017**, *442*, 72.
34. Shinde, S. S.; Jadhav, K. M.; *Mater. Lett.*, **1998**, *37*, 63.
35. Saija, K. G.; Vasoya, N. H.; Modi, S. K.; Meshiya, U. M.; Jani,K. K.; Raval, P.Y.; Modi, K. B.; *Phys. B.*, **2020**, *593*, 412302.
36. Vasoya, N. H.; Lakhani, V. K.; Sharma, P. U.; Modi, K. B.; Kumar, Ravi; Joshi,H. H.; *J. Phys.Conden. Matter.*, **2006**, *18*, 8063.
37. Rezlescu, N.; Rezlescu, E.; *Phys. Stat. Sol. (A)*, **1974**,*23*,575.
38. Perfenov, V. V.; Nazipov, R. A.; *Inorg. Mater.*, **2002**, *38*, 78.
39. https://www.enotes/homework-help/why-holes–habier-than-electrons-198147.
40. Dutta, Alo; Sinha,T. P.; Shannigrahi, S.; *J. Appl. Phys.*, **2008**, *104*, 064114.
41. Mariappan, C.R.; Govindaraj, G.; *J. Non-Cryst. Solids*, **2006**, *352*, 2727.
42. Saafan, S. A.; Seoud, A. S.;El Shater, R. E.; *Physica B*, **2005**, *365*, 27.
43. Debottom, B.; Rolling; Funke, K.; *Phys. Rev. B.*, **2000**, *63*, 024301.
44. Saija, K. G.; Ph.D. thesis, Saurashtra University, Rajkot, India, **2012**.
45. Rolling, B.; Happe, A.; Funke, K.; Ingram, M. D.; *Phys.Rev. Lett.*, **1997**, *78*, 2160.
46. Ahmad, M.M.; Yamadaand, K.; Okuda, T.; *Solid State Ionics*, **2004**, *167*, 285.
47. Gerhardt, R.; *J. Phys. Chem. Solids*, **1994**, *55*, 1491.
48. Datta, A.; Sinha, T. P.; Shannigrahi, S.; *J. Appl. Phys.*, **2008**, *104*, 064114.